Morphotropic phase transition studies in $Pb(Zr_xTi_{1-x})O_3$ by far-infrared reflectance spectroscopy

1996 J. Phys.: Condens. Matter 8 2447

(http://iopscience.iop.org/0953-8984/8/14/018)

J. Phys.: Condens. Matter **8** (1996) 2447–2456. Printed in the UK

Morphotropic phase transition studies in $Pb(Zr_xTi_{1-x})O_3$ by far-infrared reflectance spectroscopy

V Sivasubramanian†, V R K Murthy†, B Viswanathan‡ and M Sieskind§

† Department of Physics, Indian Institute of Technology, Madras - 600 036, India
‡ Department of Chemistry, Indian Institute of Technology, Madras - 600 036, India
§ Laboratoire de Physique et Applications des Semiconducteurs, CNRS, 67037 Strasbourg, France

Received 8 June 1995, in final form 25 October 1995

Abstract. The morphotropic phase transition in the $Pb(Zr_xTi_{1-x})O_3$ system has been studied by far-infrared reflectance spectroscopy. The reflectance measurements are performed on compositions with $x = 0.0$, 0.10, 0.20, 0.30, 0.35, 0.40 and 0.525 at room temperature in the frequency range 40–600 cm^{-1}. The spectrum is fitted with a model based on the factorized form of the dielectric function. The dependences of the mode frequencies, damping and oscillator strength on x are reported. The static dielectric constant is calculated from the frequencies obtained from the fitting. The observed experimental data show incomplete softening of the lowest E(1TO) mode towards the morphotropic phase boundary. The oscillator strength of the lowest mode carries nearly all the contribution to the lattice part of the dielectric constant.

1. Introduction

The $Pb(Zr_xTi_{1-x})O_3$ solid solution system at room temperature, undergoes a morphotropic phase transition in which the ferroelectric tetragonal structure transforms to a ferroelectric rhombohedral structure. This phase transition occurs at 300 K for $x = x_c = 0.53$ [1]. The elastic, piezoelectric and dielectric properties of PZT show anomalies for x-values near x_c. These anomalies are responsible for strong electromechanical behaviour and make these materials ideal for practical applications. The tetragonal–rhombohedral phase transition was described by the Landau–Devonshire thermodynamic theory which accounts for the changes in the free energy of the system with increase in the concentration of Zr [2, 3]. The theory shows that the maximum electromechanical activity near the morphotropic phase boundary is the consequence of the maximum value of the dielectric constant. However, little is known about the microscopic mechanisms which are responsible for the tetragonal–rhombohedral phase transition. Since the contribution to the dielectric constant arises partly from the polar phonon modes, it can be easily seen from the well known LST relation that, as the frequency of one of the transverse optical modes decreases, the static dielectric constant increases. Therefore it is of considerable interest to know whether the morphotropic phase transition in PZT is associated with softening of the transverse optical mode frequency. Some lattice dynamical aspects of these transitions were studied by Burns and Scott [4] using the Raman scattering technique on the powdered samples. They observed a softening of the lowest E(1TO) phonon for the composition with x up to 0.24. They could not measure the frequency of the lowest mode for $x > 0.25$ due to the low energy shift and scattering background. On the basis of the above measurements and with an additional measurement

0953-8984/96/142447+10$19.50

at $x = 0.25$, Pinczuk suggested, by extrapolation, that the square of the E(1TO) mode frequency varies linearly with x and attains zero as x approaches the critical concentration x_c [5]. However, Raman back-scattering studies on the tetragonal–rhombohedral transition revealed that the frequency of the soft mode does not go to zero at x_c [6]. One of the inherent problems in the Raman scattering spectra in perovskite oxide materials is the appearance of strong second-order lines which makes it difficult to identify the first-order modes correctly. More accurate in principle is the method of fitting the reflectivity spectra with a reasonable physical model so that a complete description of the behaviour of the mode frequencies, the oscillator strength and the damping of polar phonon modes could be achieved. Two models are generally used: the classical oscillator model and the model based on the factorized form of the dielectric function. The latter is more convenient to fit wide reflectivity bands accurately. Moreover, second-order processes do not show up in the reflectivity measurements.

In this paper, the infrared (IR) reflectivity measurements on the compositions with $x = 0.0$, 0.10, 0.20, 0.30, 0.35, 0.40 and 0.525 are reported. The mode parameters are determined accurately by fitting the experimental data with the factorized form of the dielectric function. The dependences of the frequency, the damping and the oscillator strength of each phonon together with the behaviour and dielectric constant are discussed.

2. Experimental details

The samples were prepared by the standard ceramic method. All the samples were calcined at 800 °C for 2 h and sintered in the temperature range 1150–1280 °C for 3 h. Precaution was taken to avoid PbO loss from the sample which considerably affects the far-IR spectra. PbO loss was avoided by covering the pellet with a mixture of $PbZrO_3$ and 10% ZrO_2 powder which maintains a high partial pressure over the sample. All the samples had a density in the range 96–98% of the x-ray density. Structure analyses were carried out for all samples using the Rietveld profile fitting method. The formation of a single-phase solid solution was confirmed in all cases except for $x = 0.525$, where the coexistence of both the tetragonal and the rhombohedral phases was confirmed as the rhombohedral (200) line was observed in the x-ray diffraction pattern. The variation in lattice parameters with x are shown in figure 1. The a-value increases and the c-value remains constant within the experimental accuracy. The reduction in the c/a ratio is also shown in figure 1.

The IR reflectivity spectra for all the compositions were recorded at room temperature in the frequency range 40–600 cm^{-1} at Bruker Spectrospin, Wissembourg, France, using a Bruker IFS 66v Fourier transform IR spectrometer at an angle of incidence of 11° from the normal.

3. Description of modes and ionic displacements

In the ferroelectric tetragonal phase, three triply degenerate cubic F_{1u} (IR- and Raman-active) and one triply degenerate F_{2u} (IR- and Raman-inactive) modes transform as $3A_1 + 3E$ (both are IR and Raman active) and $B_1 + E$ (the latter being IR active) irreducible representation of the C_{4v} point group. The long-range electrostatic forces split all the modes into longitudinal optical (LO) and transverse optical (TO) components. The modes that arise from the three triply degenerate F_{1u} cubic modes are labelled in sequence 1, 2 and 3 in the order of increasing frequency. For example, the three E(TO) modes are labelled E(1TO), E(2TO) and E(3TO). The same sequence is followed for A_1 symmetry modes also. The IR-inactive

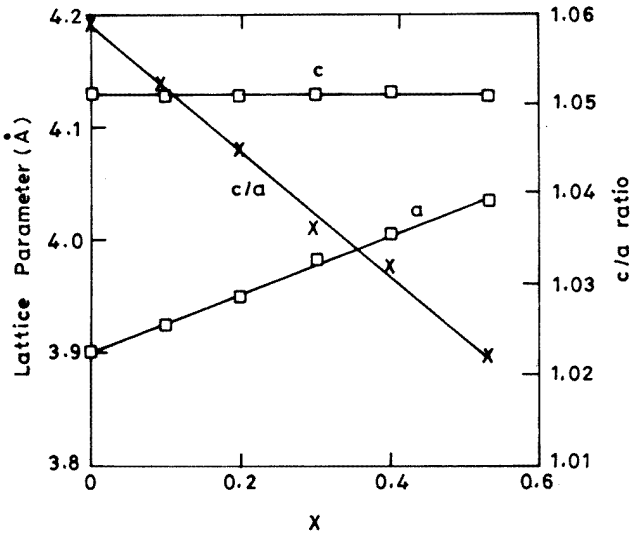

Figure 1. Variation in the lattice parameters a and c and the tetragonal distortion c/a with the composition.

F_{2u} mode is represented as a silent mode. The lowest frequency corresponds to the motion of the B ion (Ti, Zr) against the oxygen octahedron. The second frequency corresponds to a vibration of the Pb ion against BO_6 octahedra and the third consists of the motion of B and O(1) against the oxygen ions O(2) and O(3) which are located in the plane perpendicular to the direction of polarization [7]. The A_1 symmetry mode is polarized along the [001] direction (the hard direction) and the E symmetry mode is polarized in the plane perpendicular to the [001] direction (the soft direction).

4. Analysis of the data

The reflectivity spectra were fitted with the following formulae:

$$R(\omega) = \left[\frac{\sqrt{\epsilon(\omega)} - 1}{\sqrt{\epsilon(\omega)} + 1}\right]^2 \tag{1}$$

$$\epsilon(\omega) = \epsilon_\infty \prod_j \frac{\Omega_{jLO}^2 - \omega^2 + \mathrm{i}\omega\gamma_{jLO}}{\Omega_{jTO}^2 - \omega^2 + \mathrm{i}\omega\gamma_{jTO}} \tag{2}$$

where R is the reflectivity and the second relation represents the factorized form of the dielectric function arising from the generalized oscillator model [8]. Ω_{jTO} is the frequency of the TO mode, Ω_{jLO} is the frequency of the LO mode, γ_{jTO} and γ_{jLO} are the dampings of the LO and TO modes, respectively, and ϵ_∞ is the optical frequency dielectric constant. This model allows different values for the dampings γ_{jTO} and γ_{jLO} of the jth mode so that the frequency-dependent damping coefficient is taken into account in a simple form. The TO mode frequencies correspond to the peaks of the imaginary part of the complex dielectric function ϵ and the LO mode frequencies to that of the imaginary part of $1/\epsilon$. The results of the fitting are shown in figure 2. Figures 3 and 4 show TO and LO mode spectra for all the compositions.

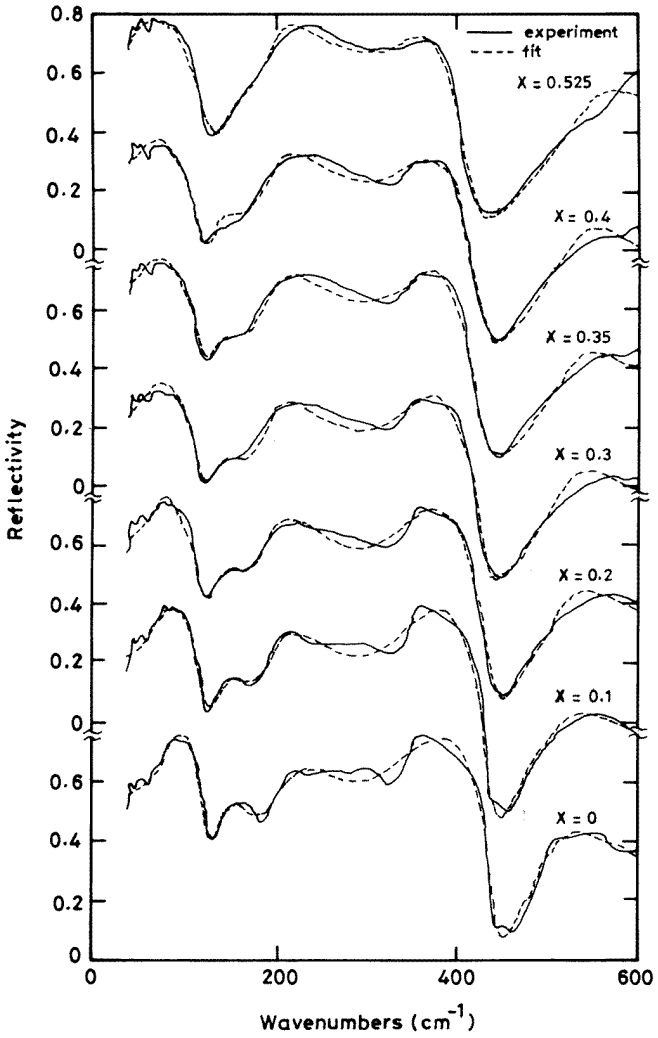

Figure 2. Reflectivity spectra of $Pb(Zr_xTi_{1-x})O_3$.

4.1. Mode frequencies

The variation in mode frequencies for all the compositions are given in figure 5. The symmetry for the modes given in figure 5 are assigned by following the symmetry assignment given for the ceramic $Pb(Zr_{0.75}Ti_{0.25})O_3$ [9]. The mode frequencies obtained in the present study for $PbTiO_3$ agree well with those from single-crystal data [10]. The symmetry of the modes for all the compositions can be easily assigned by comparing with recent IR reflectivity data reported by Zelezny *et al* [9] rather than with the data reported by Burns and Scott [10] using laser Raman spectroscopy. A silent TO mode and a silent LO mode near 350 cm^{-1} and 300 cm^{-1}, respectively, are observed for all the compositions and are shown in figure 5. It can be seen that the frequency of the lowest mode decreases towards the morphotropic phase boundary and does not become zero. This is in complete agreement with the data reported using Raman back scattering [6]. The frequency $A_1(1LO)$

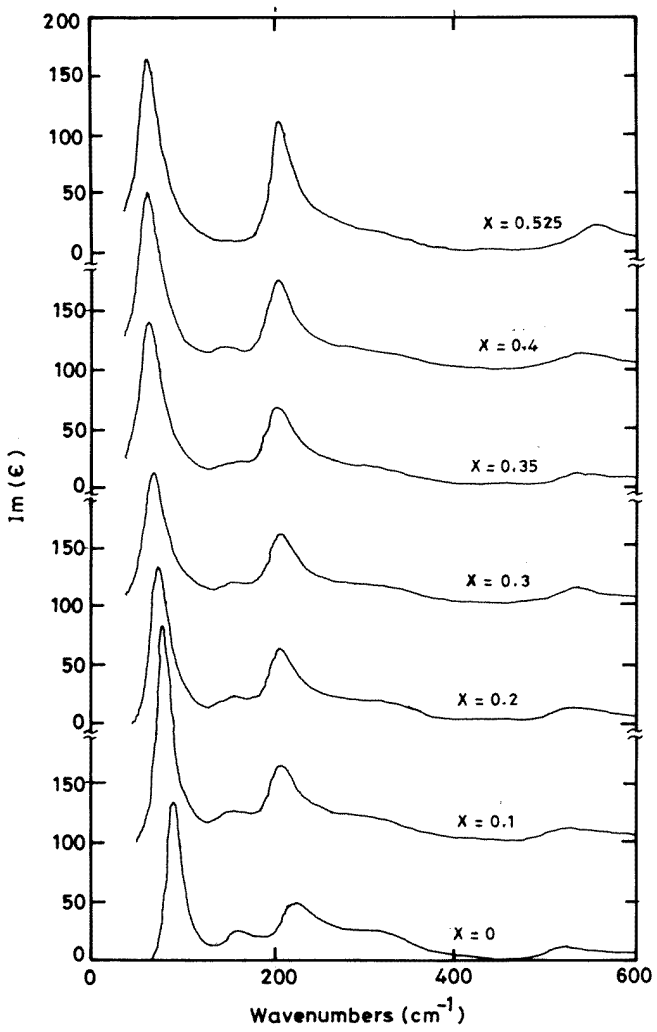

Figure 3. Imaginary part of the dielectric function (TO mode spectrum) obtained from the fit of the factorized form of the dielectric function.

and A_1(1TO) decrease slightly and have the same value at the boundary while the frequencies of all the other modes remain constant.

4.2. Oscillator strength of TO modes

The oscillator strengths of the polar modes are calculated using the following formula:

$$\Delta\epsilon_j = S_j = \epsilon_\infty \frac{\Omega_{jLO}^2 - \Omega_{jTO}^2}{\Omega_{jTO}^2} \prod_{j\neq k} \frac{\Omega_{kLO}^2 - \Omega_{jTO}^2}{\Omega_{kTO}^2 - \Omega_{jTO}^2} \tag{3}$$

Since the spectra were recorded only up to 600 cm^{-1}, we could not obtain the frequencies of the A_1(3TO), E(3LO) and A_1(3LO) modes which are present above 600 cm^{-1}. Therefore in the calculation of the oscillator strength, a constant value of frequency for these modes

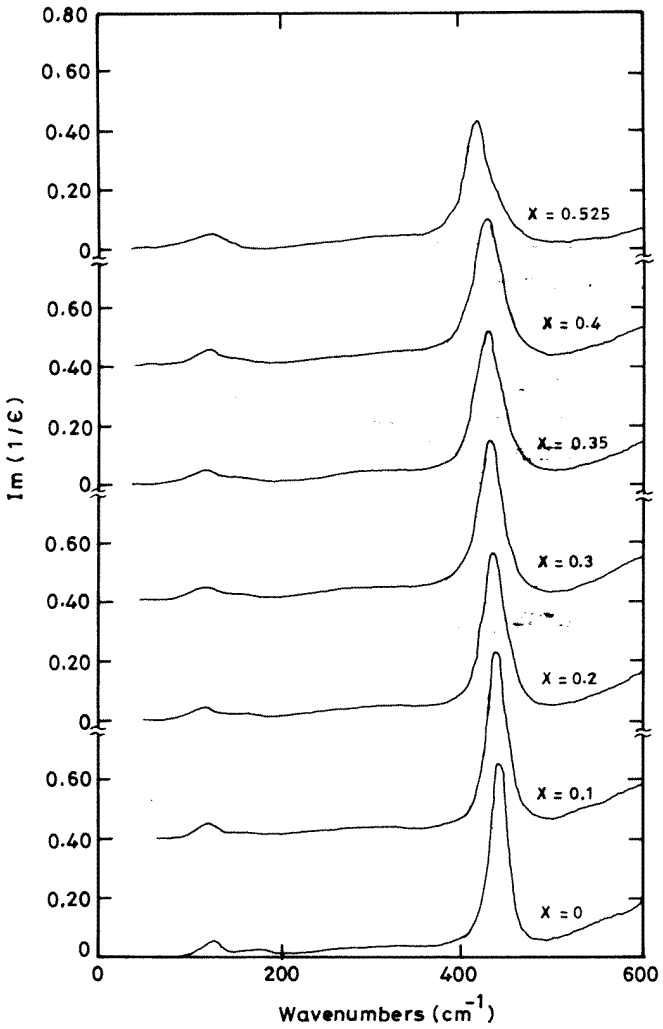

Figure 4. Imaginary part of inverse dielectric function obtained (LO mode spectrum) from the fit.

is assumed for all the compositions as the frequencies of these modes do not vary from composition to composition [4]. Values of 610 cm^{-1}, 680 cm^{-1} and 780 cm^{-1} are assumed for A_1(3TO), E(3TO) and A_1(3TO), respectively, for all the compositions in the present study. The values obtained from the above equation for all polar phonon modes as a function of x are given in figure 6. It is clearly seen that, along the soft direction considered, the oscillator strength S_1 of the soft mode shows a large increase towards the phase boundary. Although the strength S_2 is comparable to S_1 for $x = 0$, its value and the strength S_3 remain nearly the same with the composition approaching the phase boundary. Consequently, the oscillator strength S_1 carries nearly all the contributions from IR modes to the static dielectric constant of the lattice which is denoted as ϵ(lattice). The difference between the oscillator strengths along the soft and hard directions for all the modes is very large. The oscillator strength S_1 along the hard directions for all the modes is very large. The oscillator strength

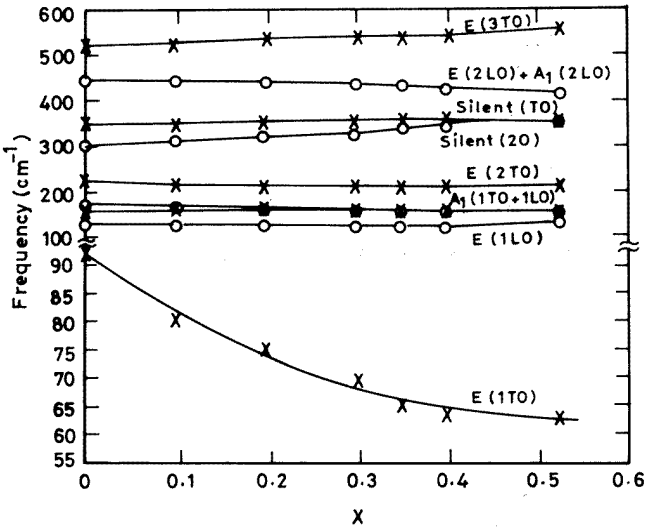

Figure 5. Variation in TO and LO mode frequencies with x.

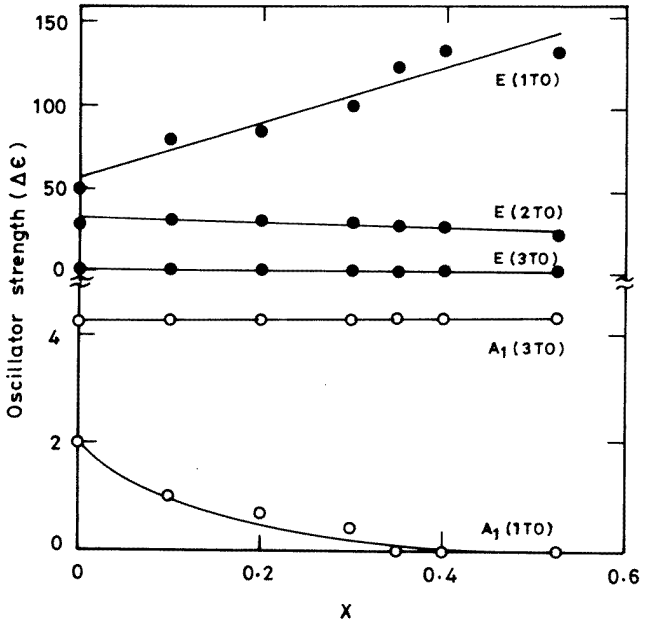

Figure 6. Variation in oscillator strength ($\Delta\epsilon$) with x.

S_1 along the hard direction diminishes to zero towards the phase boundary.

4.3. Mode damping

Figure 7 shows an increase in the damping of the soft mode towards the morphotropic phase boundary. Dvorak and Glogar [11] calculated the dependence of the soft mode on

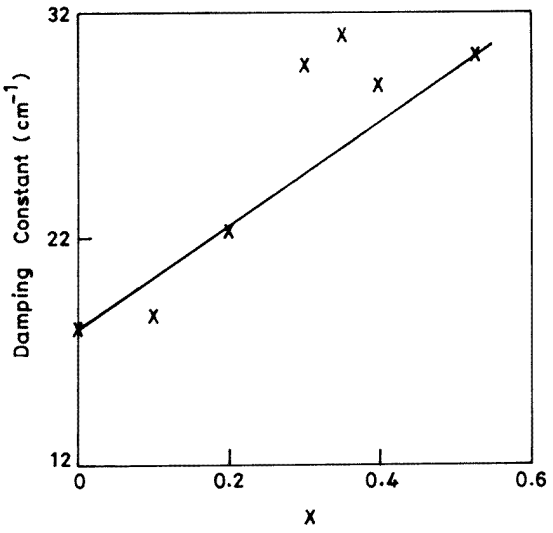

Figure 7. Variation in damping constant of the soft mode with x.

the concentration of impurities. Assuming that the change in the frequency with impurity concentration is caused only by the short-range harmonic potential, they found that

$$\omega^2(x) = \gamma\left(T_0' - T\right) \tag{4}$$

Since the long-range forces are also harmonic, their addition will not alter the form of the equation but will lead to an additional change in the critical temperature which is non-linear in x. The dependence of the critical temperature has been established experimentally and has the form

$$T_0'(x) = -117x^2 - 132x + 490 \tag{5}$$

for $0 < x < 0.52$ [6].

The calculated value of the square of the soft-mode frequency is plotted in figure 8 (broken curve). The disagreement between the calculated and the experimentally measured values leads to the conclusion that the B ion moves in an increasingly anharmonic potential towards the phase boundary. This is confirmed in the present study with the increase in the damping constant with increasing x.

4.4. Dielectric constant

The static dielectric constant ϵ(lattice) of the lattice can be derived from the Ω(TO) and Ω(LO) frequencies via the generalized LST relation

$$\epsilon_\alpha(\text{lattice}) = \epsilon_\alpha(\infty)\prod_j \frac{\Omega_j^2(\text{LO})_\alpha}{\Omega_j^2(\text{TO})_\alpha} \tag{6}$$

where α denotes the direction of the polarization axis whereas $\epsilon_\alpha(\infty)$ is the optical dielectric constant along the axis considered. Since the samples used in the present study are ceramic in nature, the complications introduced by the random orientation of crystallographic directions in the crystallites have to be taken into consideration [12].

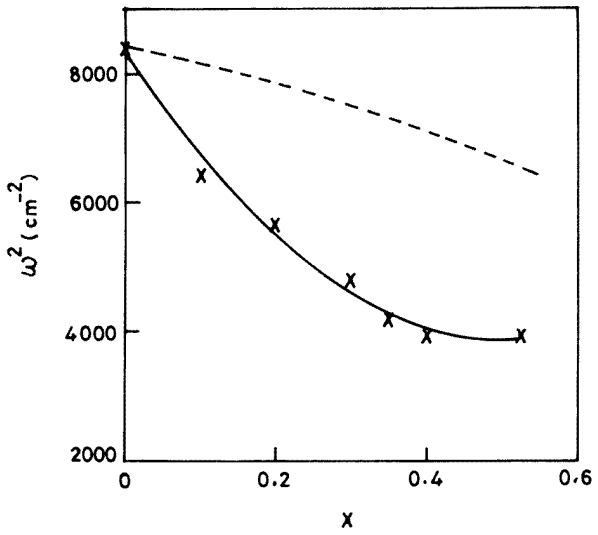

Figure 8. Variation in the square of the soft mode frequency with x. Experimental data (——) and the data calculated from equation (4) (- - - -) are shown.

Therefore an average isotropic value of dielectric constant is calculated and is compared with the experimental data. The comparison between the calculated value of the dielectric constant given by ϵ(lattice) and the experimental data given by ϵ(exp) provides a good check to know whether the morphotropic phase transition can be completely associated with the softening of the lowest phonon. The dielectric constant deduced from the LST relation takes into account only the phonon and electronic parts, whereas the experimentally measured dielectric constant exhibits several distinct regimes as a function of frequency. The experimentally measured dielectric constant strongly depends on the piezoelectric resonances, the contribution from ferroelectric domains, the structural disorder and the impurities. Therefore, in order to compare ϵ(lattice) and ϵ(exp), the experimental data ϵ(exp) have to be chosen in the clamped configuration which corresponds to frequencies well below the phonon resonance but above all mechanical resonances. PZT exhibits a piezoelectric resonance at around 250 kHz and an additional relaxation at around 700 MHz. This relaxation was found to be independent of the concentration x, and the strength of the relaxation increases with change in the composition towards the morphotropic phase boundary [13]. Since the dielectric relaxation at 700 MHz is believed to be due to the relaxation from domain walls, at frequencies above this, one expects that the domain wall contribution will die out and the major contribution to the dielectric response will be due only to the intrinsic lattice part [14]. Therefore the calculated dielectric constant is compared with the value measured at 10 GHz. Since ceramic samples are used, the average value of the dielectric constant is compared and the data are shown in table 1. Good agreement is found for $PbTiO_3$ and the discrepancy increases with change in the composition towards the phase boundary. The absence of dispersion in $PbTiO_3$ and the disagreement between the calculated and the measured values of the dielectric constant show the possibility that another relaxation above 10 GHz exists in PZT.

Table 1. Calculated average isotopic value of dielectric constant using equation (8) for all the compositions. The experimental value ϵ(exp) is taken from the references cited.

Zr concentration x	Average ϵ(lattice)	ϵ(exp) at 10 GHz
0.000	66	59 [15]
0.100	87	—
0.200	89	—
0.300	99	—
0.350	114	—
0.400	118	185 [13]
0.525	115	400 [13]

5. Conclusion

The softening of the lowest phonon mode is observed and the softening becomes incomplete at the phase boundary. The increases in the oscillator strength and the damping of the soft mode indicates that the phase transition is mainly driven by the anharmonic potential in which the B ion moves. The disagreement between the measured and the calculated values of the square of the soft mode frequency confirms this. Despite the difference between the measured and the calculated values of dielectric constant, the increases in the oscillator strength and the damping indicate that the softening of E(1TO) evidently plays an important role in the tetragonal–rhombohedral transition of $Pb(Zr_xTi_{1-x})O_3$. The difference between the calculated and the measured dielectric constants shows that additional relaxation may be present above 10 GHz in $Pb(Zr_xTi_{1-x})O_3$.

Acknowledgment

The authors are grateful to Dr J C Boulou, IRTF Department, Bruker Spectrospin, Wissembourg, France, for recording the reflectivity spectra for the samples in the present study.

References

[1] Jaffe B, Cook W R and Jaffe H 1971 *Piezoelectric Ceramics* (London: Academic)
[2] Benguigui L 1972 *Solid State Commun.* **11** 825
[3] Harl K and Hardtl K H 1971 *Phys. Status Solidi* a **8** 87
[4] Burns G and Scott B A 1970 *Phys. Rev. Lett.* **25** 1191
[5] Pinczuk A 1973 *Solid State Commun.* **12** 1035
[6] Bauerle D, Yacoby Y and Richer W 1974 *Solid State Commun.* **14** 1137
[7] Fontanna M D, Metrat G, Servoin J L and Gervais F 1984 *J. Phys. C: Solid State Phys.* **16** 483
[8] Gervais F and Piriou B 1974 *Phys. Rev.* B **10** 1642
[9] Zelezny V, Simon P and Gervais F 1987 *Mater. Res. Bull.* **22** 1695
[10] Burns G and Scott B A 1973 *Phys. Rev.* B **7** 3088
[11] Dvorak V and Glogar P 1966 *Phys. Rev.* **143** 344
[12] Stroud D 1975 *Phys. Rev.* B **12** 3368
[13] Kersten O and Schmidt G 1986 *Ferroelectrics* **67** 191
[14] Zhang Q M, Wang H, Kim N and Cross L E 1994 *J. Appl. Phys.* **1** 454
[15] Poplavko Yu M and Tyskalov V G 1967 *Sov. Phys.–Solid State* **8** 2490